Brownian Dynamics Simulations of Wormlike Chains: Dynamic Light Scattering from a 2311 Base Pair DNA Fragment

Stuart A. Allison*

Department of Chemistry, Georgia State University, Atlanta, Georgia 30303

Susan S. Sorlie and R. Pecora

Department of Chemistry, Stanford University, Stanford, California 94305.
Received June 1, 1989; Revised Manuscript Received August 23, 1989

ABSTRACT: The technique of Brownian dynamics simulation is used to study dynamic light scattering (DLS) from a linear 2311-bp fragment of DNA. A variety of different semistiff models are considered, and the simulation results are compared with actual experiments (Sorlie, S.; Pecora, R. *Macromolecules* **1988**, *21*, 1437). The parameters of the model are chosen subject to the constraints that the overall translational diffusion constant (D_0) and mean-square radius of gyration ($\langle S^2 \rangle$) match experimental values. Time correlation functions are analyzed by CONTIN, which constructs the distribution of relaxation times, and by cumulant and average lifetime methods. At $q^2 = 2.684 \times 10^{10}$ cm^{-2}, CONTIN analysis of simulations on 10 subunit chains with hydrodynamic interaction (HI) included is in better agreement with experiment than the corresponding free draining models. For the ensemble sizes employed in the simulations (300 trajectories), there is some uncertainty in the faster decay portion of the lifetime distribution. In the scattering vector range $4 \times 10^{10} < q^2 < 10^{11}$ cm^{-2}, the CONTIN analysis of models with sufficient stiffness to give the requisite $\langle S^2 \rangle$ and D_0 with HI give DLS results that are not very different from the Gaussian coil model with no HI and stiffness added indirectly via the $\langle S^2 \rangle$ and D_0 constraints. At higher values of the scattering vector, cumulant analysis is able to discriminate between models with different amounts of stiffness and the same $\langle S^2 \rangle$ and D_0. For stiff/flexible models there exists an intermediate range of scattering vector in which the first cumulant varies as q^3/q^4 for chains with and without intersubunit HI. DLS appears to be insensitive to the number of subunits in models that are subjected to similar constraints provided $q < 5.0\langle b^2 \rangle^{1/2}$ where $\langle b^2 \rangle$ is the mean-square intersubunit separation.

I. Introduction

Over the past few years, the technique of Brownian dynamics simulation[1-3] has proven very useful in the study of polymer motion in solution.[4-10] The objective of this work is to use this simulation procedure to study the polarized dynamic light scattering behavior of a monodisperse, semistiff polymer model and compare the results to those of actual experiments on a 2311-bp DNA fragment.[11] Dynamic light scattering, unlike techniques such as electric birefringence or viscoelastic dispersion and relaxation, does not perturb the macromolecule from its equilibrium environment.

A primary objective of polymer physics is to obtain a fundamental understanding of the translational, rotational, and intramolecular dynamics of macromolecules with variable stiffness. For semistiff polymers, experimental and theoretical techniques are largely undeveloped. Pecora[12] calculated the time correlation function for polarized dynamic light scattering (DLS) for a Gaussian or Rouse–Zimm model[13,14] in the free draining limit. This treatment has the advantage of mathematical simplicity but ignores hydrodynamic interaction and bending flexibility. Lin and Schurr[15] subsequently developed an algorithm for calculating the time correlation function for Rouse–Zimm chains with preaveraged hydrodynamic interaction included. Fujime and co-workers[16,17] have developed a theory for DLS from semistiff macromolecules based on the Harris–Hearst model.[18,19] This model works well near the flexible coil limit but breaks down in the rigid rod limit due to large mean-square fluctuations in the contour length of the chain. The shortcomings of the Harris–Hearst model have been pointed out in a quantitative way by Soda.[20] Stimulated by the work of Soda, Aragon and Pecora[21] developed a dynamical theory for the free draining Kratky–Porod[22] wormlike chain. However, this theory has not been applied to the problem of DLS except for a few limiting special cases. Overall, the difficulties of developing analytic theories of DLS from linear semistiff polymers remain formidable. At present, there are no adequate theoretical treatments that predict polarized DLS time correlation functions from which a distribution of relaxation times may be obtained. We circumvent this difficulty in the present work by the technique of Brownian dynamics simulation.[2,7-9]

Briefly, the DLS time correlation function is obtained by carrying out a large number of dynamical trajectories of individual chains and calculating the necessary averages corresponding to the experimental observable. The chain model used in this work is general enough to account for hydrodynamic interaction, bending and stretching flexibility, and finite chain length. These data are then analyzed by the method of cumulants[23] and by CONTIN[24] which makes it possible to obtain the model-independent distribution of relaxation times, $G(\tau)$. A comparison of simulated analyses with each other and with the experimental results then makes it possible to determine how variations in the simulation parameters affect the cumulants and the distributions of relaxation times and perhaps to choose models that best fit the experimental data. In any case, such calculations help determine the sensitivity of DLS experiments to changes in the model parameters. In the following, all models exhibit the same mean-square radius of gyration and the same translational self-diffusion coefficient—both of which are determined by experiment.[11] Thus, the models treated here are not very different, and one would expect that experiments at relatively low scattering vector length, q, would not be terribly sensitive to small variations in the other model parameters. In fact, at very low q, all models would give the same $G(\tau)$ (due solely to translational diffusion).

0024-9297/90/2223-1110$02.50/0

In general, the measured quantity in DLS consists of closely spaced relaxation times that are difficult to resolve by programs such as CONTIN except perhaps in a relatively small range of q.[11,25] Such analyses show some variation in the $G(\tau)$ from run to run due to different noise realizations both in the simulations and in the experiments. In the experiments there are also variations due to the presence of small amounts of "dust". The noise variations may mask the relatively small differences in $G(\tau)$ for the different models considered here, and these together with variations due to dust in the experiments may explain some of the differences between the models and the experiments. There are also some ambiguities in applying the proper amount of "smoothing" in the CONTIN program. To mitigate these difficulties, a systematic analysis of the full relaxation time distribution functions including studies of the peak widths and the merging of peaks should be done as a function of scattering vector length in order to extract the full amount of information contained in the data.[11] Such full analyses are not reported here because the simulation data are not accurate enough to yield reproducible CONTIN distributions in the scattering vector length region of most interest. Evidently, Brownian dynamics simulations over ensembles significantly larger than 300 independent trajectories are required in order to achieve this. CONTIN distributions are presented at $q^2 = 2.684 \times 10^{10}$ cm^{-2} for several models. This scattering vector length represents the approximate lower bound at which the CONTIN distribution of relaxation times is resolvable into multiple peaks for 2311 base pair DNA.[11] For larger q, where considerable broadening and merging of peaks has occurred, only analyses of the CONTIN peak positions and areas are considered.

Other quantities such as average lifetimes and the first cumulant appear to exhibit somewhat less variation from run to run than does a CONTIN analysis once one has chosen a standard method of computing them. The quantities obtained, however, are unlikely to be the true cumulants or average lifetimes at high q where the actual distribution of relaxation times may be wide.[26] It is useful, however, to use such numbers to characterize the DLS time correlation function after carefully specifying the method of computation. At high q we use these quantities almost exclusively.

The outline of the paper is briefly as follows. In section II, the model used to represent the linear macromolecule is discussed first followed by a description of the dynamics algorithm. This is followed by a section on data analysis where CONTIN and the cumulant method are introduced. Results are presented in section III. Cumulants are discussed first for a number of different models, and this is followed by CONTIN analyses. Cumulant and average lifetime results are then presented and discussed for a variety of models. These studies are extended to very high scattering vector in order to assess under what conditions the models we use are valid and also the potential of DLS in distinguishing different models. Section IV summarizes the main points of the paper.

II. Methods

Chain Model. In early Brownian dynamics studies of short DNA fragments,[6,7] the Hagerman–Zimm model[27] was employed. This model consists of a string of touching beads of diameter 31.8 Å with stiffness incorporated into the chain through a quadratic bending potential. Simulations of short chains and short trajectory times are feasible by using this basic model. Recent triplet anisotropy simulations[9] on a 209 base pair fragment (24 beads) and trajectory time per chain of 2.5 μs required several hours of CPU time on an Amdahl mainframe. Typically, 100 trajectories per simulation were carried out. Since CPU time varies roughly as N^aTM where N, T, and M are number of beads, trajectory times, and number of trajectories, respectively, and a ranges from 1 to 3 depending on the treatment of hydrodynamic interaction; simulations on significantly longer chains for longer trajectory times are simply not feasible. For the 2311-bp DNA fragment considered in this work, a cruder model must be used.

A more general model has been described previously[8] and is used in the present work. It consists of a linear string of N beads each of radius a connected by $N - 1$ virtual bonds with bending (U^b) and stretching (U^s) potentials

$$\beta U^b = (g/2) \sum_{j=1}^{N-2} \Theta_j^2 \tag{1}$$

$$\beta U^s = (c/2) \sum_{j=1}^{N-1} ((b_j - b_0)/b_0)^2 \tag{2}$$

where $\beta = 1/kT$ (k is Boltzmann's constant and T is absolute temperature), g is a bending force constant, Θ_j is the angle between virtual bonds j and $j + 1$, c is a stretching force constant, b_j is the length of the jth virtual bond (which is also the distance between subunits j and $j + 1$), and b_0 represents the virtual bond length corresponding to the minimum in the stretching potential for individual bonds. Defining the dimensionless force constants g and c in this way is done for convenience sake, and we do not mean to imply that they are independent of temperature.

There are five parameters in this model: N, g, c, b_0, and a. From the light scattering experiment on a 2311-bp DNA fragment, the translational diffusion constant, D_0, and rms radius of gyration, $\langle S^2 \rangle^{1/2}$, are known to be 4.56×10^{-8} cm^2/s and 1044 Å at approximately 0.1 M salt and a temperature of 20 °C.[11] *In all the simulations described in this work, model parameters are chosen to reproduce this D_0 and $\langle S^2 \rangle^{1/2}$.* For a continuous wormlike chain model with persistence length P and contour length L, $\langle S^2 \rangle$ is related to P and L by the relation[28]

$$\langle S^2 \rangle = LP/3 - P^2 + 2P^3/L - 2P^4(1 - \exp(-L/P))/L^2 \tag{3}$$

From the experimental $\langle S^2 \rangle$ and a rise per base pair of 3.4 Å, a persistence length of 500 Å can be deduced. A value of 2712 Å can also be inferred for the rms end-to-end distance, $\langle R^2 \rangle^{1/2}$, using the well-known expression[28]

$$\langle R^2 \rangle = 2LP\{1 - P/L + (P/L) \exp(-L/P)\} \tag{4}$$

Hence, this gives us an additional quantity to reproduce.

Since the number of model parameters exceeds the two or three constraints imposed by D_0, $\langle S^2 \rangle$, and (optionally) $\langle R^2 \rangle$, the number of possible models is unlimited. In this work, N and c are simply chosen. The remaining three parameters can then be uniquely determined provided three constraints are imposed. Alternatively, one can choose N, c, and certain values of g (or b_0) and then uniquely determine the remaining two parameters subject in this case to two constraints. How this is done is described below.

The mean square end-to-end distance and mean square

radius of gyration of the five-parameter model turn out to be

$$\langle R^2\rangle = (N-1)\langle b^2\rangle + 2\langle b\rangle^2\alpha(1-\alpha)^{-1}\{(N-2) - (\alpha-\alpha^{N-1})(1-\alpha)^{-1}\} \quad (5)$$

$$\langle S^2\rangle = (N-1)(N+1)(6N)^{-1}\{\langle b^2\rangle + 2\alpha\langle b\rangle^2(1-\alpha)^{-1}\} - \alpha(N-1)\langle b\rangle^2\{N(1-\alpha)^2\}^{-1} + 2\alpha^2\langle b\rangle^2\{N^2(1-\alpha)^3\}^{-1}\times\{(N-1) - (\alpha-\alpha^N)(1-\alpha)^{-1}\} \quad (6)$$

where

$$\alpha = \langle\cos\theta\rangle = \int_0^\pi \cos\theta\sin\theta\exp(-g\theta^2/2)\,d\theta \Big/ \int_0^\pi \sin\theta\exp(-g\theta^2/2)\,d\theta \quad (7)$$

$$\langle b^m\rangle = \int_0^\infty b^{m+2}\exp[-c(b/b_0-1)^2/2]\,db \Big/ \int_0^\infty b^2\exp[-c(b/b_0-1)^2/2]\,db \quad (8)$$

In the limit g is much greater than 1, eq 7 simplifies to $\alpha = 1 - 1/g$. For the chains considered in the present work, however, this limiting case is not valid. Nonetheless, it is straightforward to integrate eq 7 numerically and construct a table which relates α and g. In the limit c is much greater than 1, eq 8 can be solved for $\langle b\rangle$ and $\langle b^2\rangle$ to yield b_0 and $b_0^2(1-1/c)$, respectively. Again, eq 8 can be integrated numerically for general cases. When $c = 100$ (a case used frequently in this work), exact and approximate $\langle b^2\rangle$'s deviate from each other by 3.8%. In the present work, the large c limit is assumed valid provided $c \geq 100$. Otherwise, eq 6 is solved numerically to relate $\langle b^m\rangle$ to c and b_0.

Once N and c are chosen, the parameters b_0 and g can be determined by iterative solution of eq 5–8. Alternatively, N, c, and g can be chosen and b_0 uniquely determined if the $\langle R^2\rangle$ constraint is ignored. In either approach, all model parameters except a (bead radius) are either selected or determined.

The one remaining model parameter (a) is determined by the constraint of D_0. This, in turn, depends on the assumed model of hydrodynamic interaction between the subunits. In the absence of hydrodynamic interaction (the free draining limit), D_0 is simply related to the subunit diffusion constant, D_s, by

$$D_0 = D_s/N \quad (9)$$

where $D_s = kT/6\pi\eta a$ and η is the solvent viscosity. In those cases where hydrodynamic interaction is included, the algorithm of Garcia de la Torre and co-workers[29] is used to compute the translational diffusion tensor $\mathbf{D}_T$, for an ensemble (500–2000) of chains with variable a (the other four parameters have been selected or determined at this point). By iteration, the bead radius that reproduces D_0 ($D_0 = \mathrm{Tr}(\mathbf{D}_T)/3$ where Tr represents the trace) is determined. In the algorithms for computing $\mathbf{D}_T$ as well as Brownian dynamics, the hydrodynamic interaction (HI) tensors between subunits i and j, $\mathbf{D}_{ij}$, are needed. These tensors are approximated using the Rotne–Prager tensor.[30] For $i = j$

$$\mathbf{D}_{ii} = (kT/6\pi\eta a)\mathbf{I} \quad (10)$$

where $\mathbf{I}$ is the 3 by 3 identity tensor. For different but nonoverlapping beads

$$\mathbf{D}_{ij} = (kT/8\pi\eta r_{ij})\{\mathbf{I} + \mathbf{r}_{ij}\mathbf{r}_{ij}/r_{ij}^2 + (2a^2/r_{ij}^2)(\mathbf{I}/3 - \mathbf{r}_{ij}\mathbf{r}_{ij}/r_{ij}^2)\} \quad (11)$$

where $\mathbf{r}_{ij} = \mathbf{r}_i - \mathbf{r}_j$ and $r_{ij} = |\mathbf{r}_{ij}|$. For overlapping beads ($r_{ij} < 2a$)

$$\mathbf{D}_{ij} = (kT/6\pi\eta a)\{(1 - 9r_{ij}/(32a))\mathbf{I} + 3\mathbf{r}_{ij}\mathbf{r}_{ij}/(32ar_{ij})\} \quad (12)$$

Dynamic Simulation. The technique of Brownian dynamics is ideally suited to study the time evolution of model polymer chains in solution.[1-3] In this work, the Ermak–McCammon algorithm is used.[2] Let $\mathbf{r}_i^0$ denote the position of subunit i at the start of a dynamics step of duration Δt. Its position after the dynamics step is given by

$$\mathbf{r}_i = \mathbf{r}_i^0 + \beta\Delta t\sum_{j=1}^{N}\mathbf{D}_{ij}^0\mathbf{f}_j^0 + \mathbf{s}_i(\Delta t) \quad (13)$$

where $\mathbf{f}_j^0$ is the initial direct force on subunit j, $\mathbf{s}_i$ is a vector of Gaussian random numbers of zero mean, and variance-covariance

$$\langle\mathbf{s}_i\mathbf{s}_j\rangle = 2\mathbf{D}_{ij}^0\Delta t \quad (14)$$

and $\mathbf{D}_{ij}^0$ is the HI tensor between subunits i and j evaluated at the start of the dynamics step. When HI is included in the simulations, eq 10–12 are used to calculate $\mathbf{D}_{ij}^0$. In the free draining limit, $\mathbf{D}_{ij}^0$ is given by eq 10 but all $i \neq j$ terms are set to zero. In most of the simulations where HI is included, the interaction tensors are orientationally preaveraged. In this case, $\mathbf{D}_{ij}^0$ in eq 13 is replaced with

$$(\mathbf{D}_{ij}^0)_{opa} = \mathrm{Tr}\langle\mathbf{D}_{ij}\rangle/3 \quad (15)$$

where $\langle\ \rangle$ denotes the average over 500–2000 different starting configurations selected from an equilibrium distribution of chains.

To simulate a polarized dynamic light scattering experiment, the dynamic scattering form factor[31]

$$S(q,\tau) = N^{-2}\langle\sum_{i=1}^{N}\sum_{j=1}^{N}\exp[-i\mathbf{q}\cdot(\mathbf{r}_i(t) - \mathbf{r}_j(t+\tau))]\rangle \quad (16)$$

is computed where $\mathbf{q}$ is the scattering vector of magnitude

$$q = (4\pi n/\lambda)\sin(\theta/2) \quad (17)$$

n is the index of refraction (set to 1.3334), λ is the wavelength of scattered light, and θ is the scattering angle. The usual Rayleigh–Debye approximation is made that the polarizability of the macromolecule is the sum of the polarizabilities of the individual subunits which comprise it. Also implicit in the use of eq 16 is the approximation that the subunits, which in this work are actually spheres of radius a, can be treated as point scatterers of light. This "point scattering approximation" and the more general Rayleigh–Debye approximation work well at low q, but for $qa > 1$ there is significant destructive interference from light scattered from different portions of the same subunit. Because of this, eq 16 is only valid for $qa < 1$. In a single simulation, several hundred dynamical trajectories are carried out in order to evaluate the average in eq 16 for a range of different q's. Ideally, the trajectory time, t_{max}, should be chosen large enough so that $S(q,t_{max})$ has decayed to within a few percent of its initial value. This is necessary to obtain a satisfactory fit to the data when the CONTIN program discussed in the next section is used. At large q, this poses no problem but at small q, where $S(q,t)$ decays away with a lifetime that varies (roughly) as q^{-2} only partial decay is possible. In the simulations reported here, the longest t_{max} is 3000 μs. At $q^2 = 2.684\times10^{10}$ cm^{-2} ($\theta = 57°$,

λ = 488 nm) Sorlie and Pecora observed a 823-μs longest relaxation time for 2311-bp DNA[11] so $S(q,t)$ should decay to about 2.6% of its initial decay in 3000 μs under these conditions. In this work, CONTIN analysis is only carried for $q^2 \geq 2.684$ or 4.171×10^{10} cm^{-2} depending on the model. Cumulant analysis is carried out at smaller q, however.

Data Analysis. Simulation results are analyzed by using a versatile, model independent data analysis program called CONTIN developed by Provencher and coworkers[24] and the cumulant method.[23,26] Define the normalized dynamic scattering form factor

$$g(t) = S(q,t)/S(q,0) \tag{18}$$

In this work, CONTIN is used to fit $g(t)$ to a continuous distribution of relaxation times

$$g(t) = \int_0^\infty G(\tau) \exp(-t/\tau)\, d\tau \tag{19}$$

where $G(\tau)$ is a normalized distribution function and τ is the relaxation time. In the special case of a monodisperse sample at low q, where overall rotation and internal motion of the macromolecule do not contribute to the decay, $G(\tau) = \delta(\tau - 1/q^2D_0)$ where δ denotes the delta function and D_0 the translational diffusion constant. Subject to the constraint that $G(\tau)$ is nonnegative, CONTIN finds the simplest form of $G(\tau)$ that adequately fits the data. In general, this is an ill-posed problem since many possible solutions exist that fit the data within experimental error. In CONTIN, the problem is formulated as a weighted least-squares fit with an added quadratic term, the regularizor, which imposes parsimony (smoothness). The regularizor along with statistical prior knowledge ($G(\tau) \geq 0$) greatly limits the range of acceptable solutions. In Brownian dynamics, an overall simulation (of 300 trajectories, for example) is broken down into subsimulations (5 subsimulations of 60 trajectories each, for example). From the range observed in $g(t)$ in the subsimulations, the standard deviations can be determined. This typically amounts to 0.002–0.004 in $g(t)$. In order to check the reproducibility of the CONTIN fits, Gaussian random noise with standard deviations in this magnitude range is repeatedly added to the simulated data. In general, if the data is relatively noisy, CONTIN fits the data to a smoother, broader $G(\tau)$ and is less likely to resolve decay processes that are close together. For more discussion and detail regarding CONTIN, the reader is referred elsewhere.[8,11,24,25]

In the cumulant method,[23,26] the logarithm of $g(t)$ is written

$$\ln g(t) = -K_1 t + K_2 t^2/2 - K_3 t^3/6 + \ldots \tag{20}$$

where K_i is the ith cumulant. The first cumulant can be expressed as

$$K_1 = \langle 1/\tau \rangle = \int_0^\infty \tau^{-1} G(\tau)\, d\tau \tag{21}$$

where τ and $G(\tau)$ have the same meaning as in eq 19. For a monodisperse sample at sufficiently small q, $K_1 = q^2D_0$ and all higher cumulants vanish. For a flexible macromolecule like DNA, however, the number of relaxation processes increases as q increases and also the number of nonvanishing cumulants. In this work as in the experiments,[11] only the first two cumulants in eq 20 are retained in a least-squares fit to the data. In the simulations, the fit is further restricted to those data points with $g(t) \geq 0.01$. Because of these restrictions, eq 21 is no longer strictly valid. Also, the calculated value of K_1 becomes somewhat dependent on the delay time between data points and the number of data points in the cumulant fit.[26,32] K_1 can also be obtained from CONTIN since $\langle 1/\tau \rangle$ is tabulated in the output.[11] Unfortunately, there is considerable uncertainty in $\langle 1/\tau \rangle$ when simulated Brownian dynamics data is analyzed. This can be understood as follows. In general, $g(t)$ consists of a distribution of relaxation times consisting of fast and slow components. The amplitudes and lifetimes of the slow components are fairly robust whereas the amplitudes and lifetimes of the fast components vary significantly from one independent simulation to the next. This can also be demonstrated by simply changing the seed to the random number generator that adds Gaussian random noise to simulated or experimental data. In the case of $\langle 1/\tau \rangle$, small amplitudes of fast components make a significant contribution to the average. A more convenient quantity is the reciprocal of the average lifetime that will be defined as K_p

$$K_p = 1/\langle \tau \rangle = 1/\int_0^\infty \tau G(\tau)\, d\tau \tag{22}$$

which is tabulated in the CONTIN output. Not only is this quantity more reproducible as far as simulations are concerned, it is also relatively insensitive to the delay time in $g(t)$ and number of data points that CONTIN fits. In actual light scattering experiments, however, K_p has the disadvantage that it is more sensitive to dust than K_1. In the special case of a single relaxation process $K_1 = K_p$. In section III, all K_1 values have been determined by least-squares fit to eq 20 (only K_1 and K_2 terms retained) and K_p from eq 22 and CONTIN.

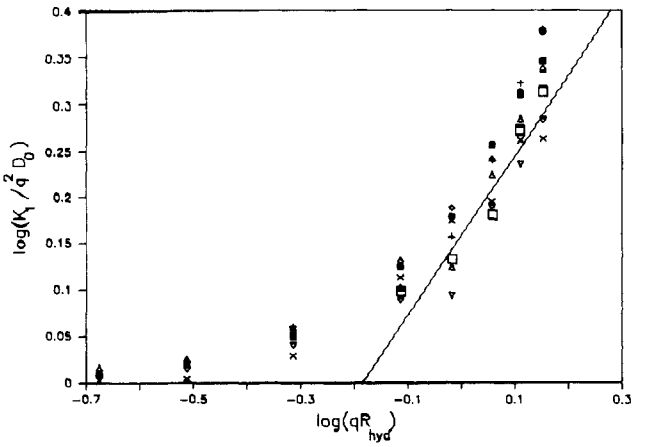

Figure 1. Dependence of K_1 on q for various models of 2311-bp DNA. Log scales are in base 10. Model parameters below are in the order no HI/HI, N, a (Å), b_0 (Å), c, and g: (■) no HI, 10, 46.7, 550, 100, 1.31; (+) no HI, 10, 46.7, 808, 100, 0.00; (◇) no HI, 10, 46.7, 668, 10, 0.00; (△) no HI, 20, 23.6, 320, 100, 1.83; (×) HI, 10, 82, 550, 100, 1.31; (□) HI, 10, 77, 668, 10, 0.00; (▽) HI, 20, 45, 320, 100, 1.83.

III. Results and Discussion

The dependence of simulated first cumulants on scattering angle (θ=15–123° with λ = 488 nm) are plotted in Figure 1 for a variety of different models. R_{hyd} = 470.4 Å corresponds to the effective hydrodynamic radius of the macromolecule and is related to D_0 by Stokes law. The solid line, which has a slope of 0.85, represents experimental cumulant data[11] at the higher scattering angles studied ($\theta \geq 90°$). This slope implies a dependence of K_1 that varies roughly as q^3 which is also the power law dependence of a long Rouse–Zimm coil in the nonfree draining limit.[33] It is evident that simulated and experimental cumulants are in fairly good agreement with each other. Experimental cumulants tend to fall between model

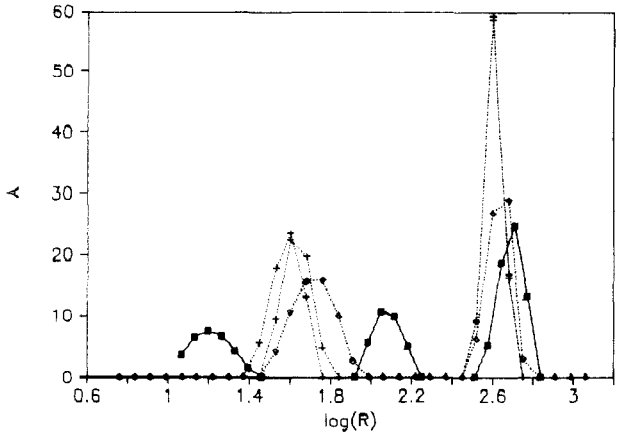

Figure 2. CONTIN analysis at $q^2 = 2.684 \times 10^{10}$ cm^{-2}: Comparison of experiment with free draining subunit models. R is the effective hydrodynamic radius in Å and is related to the relaxation time, τ, by $R = q^2kT\tau/6\pi\eta$. The log is in base 10, and A represents amplitude in arbitrary units. The solid line and filled squares denote experimental results from ref 11 on 2311-bp DNA, and dotted lines denote simulations. Diamonds (◊)/+ symbols correspond to the same model parameters as +/filled square symbols in Figure 1.

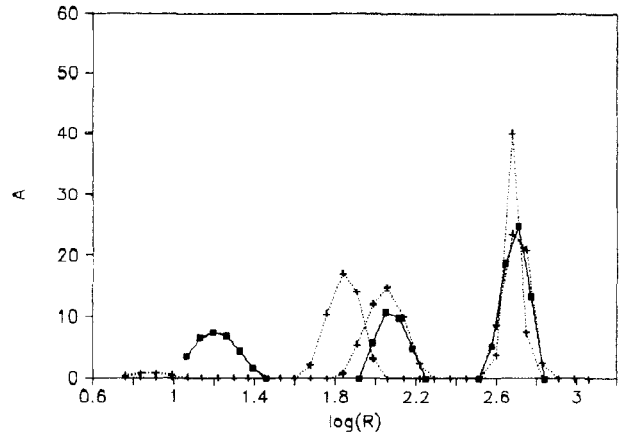

Figure 3. CONTIN analysis at $q^2 = 2.684 \times 10^{10}$ cm^{-2}: Comparison of experiment and a model with preaveraged HI. Similar to Figure 2. +'s correspond to same model parameters as ×'s in Figure 1.

values without and with HI, respectively. If no HI (free draining) model results for $\theta = 90°$ and higher are averaged and fitted by least squares, a slope of 1.16 is obtained. Although this implies a slightly stronger power law dependence than observed experimentally ($K_1 \propto q^{3.16}$), it falls significantly short of the q^4 dependence expected for a long free draining Rouse–Zimm coil.[33] For 9.105×10^{10} cm$^{-2} \geq q^2$ ($0.15 \geq \log(qR_{hyd})$), the difference between HI and no HI models are not as large as one might have expected. It is also evident that the first cumulant is insensitive to other parameters such as the bending and stretching force constants subject to the beforementioned constraints on D_0, $\langle S^2 \rangle$, and optionally $\langle R^2 \rangle$. (The 10 and 20 subunit models with $g = 1.31$ and 1.83, respectively, satisfy the $\langle R^2 \rangle$ constraint.) These results imply that the first cumulant depends primarily on overall conformation (constraint on $\langle S^2 \rangle$) and overall translational transport (constraint on D_0) at low q.

The question we would now like to address is whether or not the actual distribution of decay times, $G(\tau)$, determined by CONTIN, can help discriminate between the different models studied. Shown in Figure 2 are simulated CONTIN distributions for several free draining 10 subunit models (dotted lines) and the corresponding experimental distribution for 2311-bp DNA[11] (solid line) at $q^2 = 2.684 \times 10^{10}$ cm^{-2}. In each simulation, 300 trajectories were carried out and the + symbols correspond to $g = 1.31$ (other parameters are the same as the filled squares in Figure 1) and the diamonds to $g = 0.0$ (other parameters are the same as the + symbols in Figure 1). Results of two identical but independent simulations with $g = 1.31$ are shown to indicate the reproducibility of the distribution. The distribution of both models are not that different from each other, and although they reproduce the experimental long time peak at log $(R) \approx 2.6$–2.7, which corresponds to overall translation, the faster relaxations at smaller R are not in good agreement with experiment. Shown in Figure 3 are the corresponding results for a model with preaveraged HI. As before, dotted lines denote simulations with $g = 1.31$ (other parameters are the same as the ×'s in Figure 1) and the solid line denotes the experimental distribution. Also, the results of two identical but independent simulations (300 trajectories each) are included to indicate reproducibility. Although independent simulations are able to reproduce the long lifetime peak, there is considerably larger uncertainty in the faster peak. This uncertainty is undoubtedly due to the ensemble size of the simulations. CONTIN analyses of independent experimental data at this q were more reproducible than the simulations.[11] Nonetheless, in comparing Figures 2 and 3, it can be concluded that bead models with stiffness and HI are in better agreement with experiment than the corresponding free draining model. Previously,[11] it was shown that free draining Rouse–Zimm chains are in better agreement with experiment than the corresponding nondraining R–Z model. What the present simulations appear to show is that models that include HI and stiffness are in better agreement with experiment than models that include only one of these (e.g., R–Z nondraining or bead model with stiffness but no HI). The free-draining R–Z chain with experimentally determined $\langle S^2 \rangle$ and D_0 mimics the effects of both HI and stiffness since it gives faster "second peaks" than R–Z nondraining chains and slower second peaks compared to the no HI, 10 subunit simulations.

CONTIN analyses at larger q are summarized in Table I, where the amplitudes (A) and effective hydrodynamic radii (R) of the peaks which make up $G(\tau)$ are listed. R is related to the average lifetime of a particular peak, $\langle \tau \rangle'$, by

$$R = q^2kT\langle \tau \rangle'/6\pi\eta \tag{23}$$

The first entry in Table I summarizes the experimental CONTIN fits and the remaining entries correspond to various model fits. All model data with the exception of the free draining Gaussian coil were obtained by Brownian simulation. The Gaussian coil results were presented previously.[11] In the analysis of the Brownian simulation data, the first 31 data points of $g(t)$ had a time resolution of 2 μs and the remaining data points had a time resolution of 15 μs. Also, the longest time ($t = t_{max}$) data point in $g(t)$ was chosen sufficiently large to ensure that t_{max} equalled or exceeded three times the longest peak relaxation time in $G(\tau)$. As can be seen from the table, the model amplitudes and lifetimes are in qualitative agreement with experiment. In most cases, two or three relaxation times are observed with the largest amplitude peak corresponding to the largest R. Although obvious quantitative differences are seen between different entries, it is difficult to discern any pattern to the data which would lead one to favor one model over any of the others. The A's and R's listed denote averages of sev-

Table I
CONTIN Fits to 2311 Base Pair DNA

	73°		90°		106°		123°	
case	A	R	A	R	A	R	A	R
experiment	86	435	88	318	88	296	91	268
	16	116	10	69	10	58	5.4	69
	2.2	14	2	18			3.6	16
Gaussian coil	84	410	84	343	92	267	76	338
	16	92	16	79	8	54	20	105
no HI							4	17
$N = 10$, $a = 46.7$	84	370	79	340	65	358	55	283
$b_0 = 668$, $c = 10$	14	56	19	59	31	83	40	81
$g = 0.0$, no HI	2	2.1	2	6.3	4	9.7	5	10
$N = 10$, $a = 46.7$	73	468	62	431	100	268	100	228
$b_0 = 808$, $c = 100$	27	105	36	114				
$g = 0.0$, no HI			2	12				
$N = 10$, $a = 46.7$	100	362	82	335	75	323	61	320
$b_0 = 550$, $c = 100$			17	75	23	84	35	107
$g = 1.31$, no HI			3	6.1	2	9.7	5	12
$N = 20$, $a = 23.6$	89	377	80	355	72	342	66	322
$b_0 = 320$, $c = 100$	11	49	19	67	26	85	31	86
$g = 1.83$, no HI			1	3.8	2	8.1	3	9.8
$N = 10$, $a = 77$	74	493	56	496	78	331	82	291
$b_0 = 668$, $c = 10$	25	136	42	164	19	104	15	72
$g = 0.0$, HI	1	8.8	3	16	3	18	3	17
$N = 10$, $a = 82$	91	368	84	358	90	321	89	305
$b_0 = 550$, $c = 100$	8	55	15	95	10	60	10	79
$g = 1.31$, HI	1	8.9	1	6.3			1	5.9
$N = 20$, $a = 45$	87	413	80	391	68	381	60	367
$b_0 = 320$, $c = 100$	13	73	20	95	29	126	38	141
$g = 1.83$, HI					3	13	2	15

eral independent CONTIN fits (in most cases, independent simulations as well as just independent added Gaussian noise). In the case of the low A, smaller R peaks, variation in A and R between fits can amount to 5–40% of the average values. Hence, much of the variation in the table is probably due to noise. It should also be emphasized that $G(\tau)$ consists of broad rather than sharp peaks.[11] The change in the number of peaks for a given model as θ changes reflects the coalescence of two into a single broad peak or vice versa. There does appear to be one significant difference between experiment and most of the model studies. The models tend to show a larger amplitude of the second peak than observed experimentally. This cannot be due to the fact that the experiments were carried out at finite concentration, since high concentration tends to increase the amplitude of the second peak.[11] Also, shot noise present in experiments would be expected to incrase the amplitude of the second and higher order peaks. One possible explanation is the presence of trace amounts of dust in light scattering experiments. When a small (comparable to the noise level) amplitude component of a gradual exponential decay is added to simulated $g(t)$ data, mimicking the effect of dust, the CONTIN distribution function can be significantly altered.

In summary, CONTIN results at $q^2 = 2.684 \times 10^{10}$ cm^{-2} show that 10 subunit models with HI are in better agreement with experiment than their corresponding free draining counterparts. At larger q, however, the different constrained models with variable stiffness and HI appear to represent the data reasonably well except for minor amplitude and position variations of the second peak. Beyond that is is not possible to choose one model over the other on the basis of the present simulations. It was previously shown[11] that a full CONTIN analysis of the experiments gave closer agreement with the free draining Rouse model than with the Rouse–Zimm model with HI (all with the same $\langle S^2 \rangle$ and D_0). Adding stiffness as in the present discrete simulations appears to make HI models more consistent with the experimental results. For $4 \times 10^{10} < q^2 < 10^{11}$ cm^{-2}, we have shown that the models of the 2311-bp DNA fragment described here give similar cumulants and CONTIN peak positions and areas. This is hardly surprising since the models are not very different, and this region is not very sensitive to very local motions. Furthermore, in the CONTIN analyses, considerable merging and broadening of peaks has probably already occurred further obscuring differences among the models.[11] If calculations are performed allowing $\langle S^2 \rangle$ to vary, CONTIN and cumulant analyses of simulated data usually show very large variations as the chain conformation varies from Gaussian coil to rigid rod (keeping D_0 constant).[34] Attention will now be turned to behavior at even larger q, where we expect greater variations between the highly constrained models.

At this point, it is worthwhile to digress briefly and review some of the main features of known cumulant behavior of Rouse (free draining Gaussian) and Rouse–Zimm chains.[33,35-37] Although these models are simpler and less detailed than those studied here, they should be qualitatively similar. At very low ($q^2\langle S^2 \rangle \ll 1$) and very high ($q^2\langle b^2 \rangle \gg 1$) scattering vector length, the first cumulant appears to exhibit "plateau" behavior with $K_1/q^2 = D_0$ (low q^2) and D_s (high q^2), respectively. For sufficiently long chains, these exists a universal regime ($q^2\langle b^2 \rangle \ll 1 \ll q^2\langle S^2 \rangle$) where K_1 is independent of any property of the molecule itself. For a free draining Rouse chain, $K_1 \propto q^4$ and for a long ($N \to \infty$) Rouse–Zimm chain with preaveraged HI[35]

$$K_1 = kTq^4\langle b^2 \rangle [1 + 2(6\pi)^{1/2}B/(q\langle b^2 \rangle^{1/2})]/12\zeta \quad (24)$$

where ζ is the subunit friction factor ($\zeta = 6\pi\eta a$ from Stokes law) and B is the draining parameter

$$B = \zeta/\pi\eta(6\pi\langle b^2 \rangle)^{1/2} \quad (25)$$

Typically, the B term in parentheses in eq 24 is much greater than 1 which leads to $K_1 = kTq^3/6\pi\eta$. Universal q^3 behavior has been observed for polystyrene in a number of different solvents.[35] For DNA, on the other hand, universal behavior may not be exhibited even for fairly large fragments ($M < 10^7$ g/mol) because of the considerable stiffness of the molecule. Schurr has investigated the boundaries of the universal q^3 regime for Rouse–Zimm chains and determined that it must fall within $q^2\langle S^2 \rangle > 7$ and $q^2\langle b^2 \rangle < 0.54$.[36] For the chains studied in this work (taking $\langle b^2 \rangle^{1/2} = 500$ Å as a typical value) lower and upper bounds of $q^2 > 6.4 \times 10^{10}$ cm^{-2} and $q^2 < 2.2 \times 10^{10}$ cm^{-2} can be imposed. Note that this is only approximate since the chain model considered in this work is not Rouse–Zimm. These two conditions cannot be satisfied simulataneously that implies no universal behavior for the model chains studied in this work. One could argue that the lower bound on q^2 could be raised by increasing the number of subunits that would necessitate reducing $\langle b^2 \rangle$ because of the constraints. In this procedure, however, the model becomes progressively less Rouse–Zimm-like in character and the validity of using the criteria (established for RZ chains) progressively more uncertain. On the other hand, the upper bound on q^2 can be raised substantially if *nonuniversal* or apparent q^3 behavior is allowed.[36] Taking this upper bound to be $q^2\langle b^2 \rangle < 18.3$, $q^2 < 73 \times 10^{10}$ cm^{-2}. This is an important point from a structural standpoint since it implies that differences in K_1 over the range $6 \times 10^{10} < q^2 < 70 \times 10^{10}$ cm^{-2} may actually reflect structural and dynamical differences in model and experimental studies.

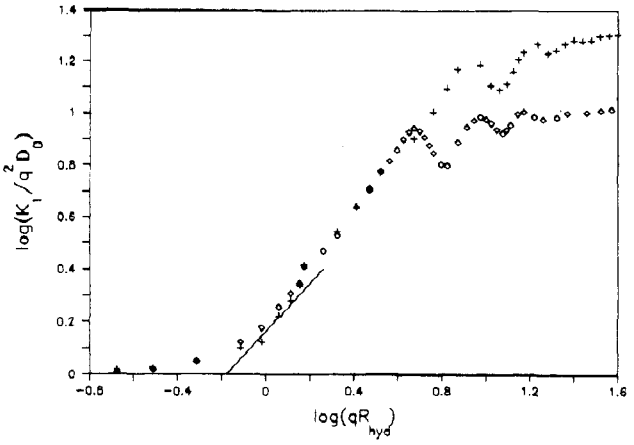

Figure 4. Effect of bead number on K_1 and for free draining chains. Solid line represents experimental cumulants. Diamonds correspond to K_1 for $N = 10$ (other parameters the same as filled squares in Figure 1). Crosses correspond to K_1 for $N = 20$ (other parameters same as triangles (△) in Figure 1).

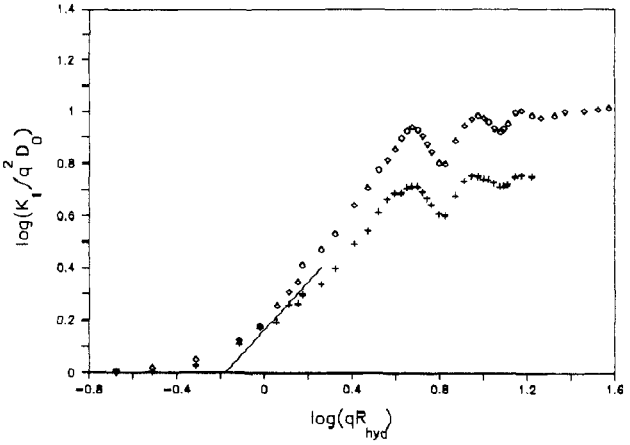

Figure 5. Effect of hydrodynamic interaction on K_1 for $N = 10$ chains. Solid line represents experimental cumulants. Diamonds correspond to K_1 for the no HI case (same as diamonds in Figure 2). Crosses correspond to K_1 for the case with preaveraged HI (parameters the same as the ×'s in Figure 1).

Figure 4 is a log–log plot (base 10) of K_1 versus q for two free draining "stiff" chains containing 10 and 20 subunits. The sloped solid line again represents the experimental K_1. For q^2 less than about 70×10^{10} cm^{-2}, the 10 and 20 subunit chains are indistinguishable. From the near linear regime ($0.0 < \log(qR_{hyd}) < 0.6$) a slope of 1.10 is deduced that corresponds closely to a q^3 dependence of K_1 (the experimental slope is 0.85). This is in excellent agreement with the power law dependence of K_1 from both experiment and model studies. It is, however, at variance with the q^4 power law dependence of a free draining Rouse chain in the universal region.[35] As discussed below, bending stiffness appears responsible for this discrepancy. At very high q, K_1 exhibits complex oscillatory behavior that, as discussed later, is a function of b_0 and c. Similar oscillations have been reported previously for simple models of supercoiled DNA.[38] At sufficiently high q, K_1 eventually plateaus and appears to approach the limiting value of q^2D_s. Finite Rouse–Zimm chains exhibit similar plateau behavior, but the peculiar oscillations seen in Figure 4 are absent.[15,35] This plateau behavior appears to be a function of the number of model subunits, their mean separation, and their size. If a more detailed 40 subunit model were studied, it would most likely coincide with the coarser 10 and 20 subunit models up to some q value, then branch off from first the 10 and then the 20 subunit models, then oscillate, and eventually reach a new and higher plateau.

The effect of preaveraged HI is shown in Figure 5. This is the same kind of plot as Figure 4 with crosses and diamonds denoting K_1's for preaveraged HI and free draining chains, respectively. Except for the model of HI and the bead radii in the two cases, the chain parameters are identical. (The no HI K_1 points also appear in Figure 4.) Again the experimental K_1 data are denoted by the sloped line. In the linear regime ($0.1 < \log(qR_{hyd}) < 0.5$), the HI data points have a slope of approximately 1 which corresponds to a q^3 dependence of K_1. This slope is comparable to the no HI case, but note from Figure 5 the HI curve falls significantly below the no HI curve at large q. At sufficiently low q, $K_1 = q^2D_0$ which accounts for the initial zero slope of K_1 in Figures 4 and 5. At higher q, K_1 exhibits a stronger dependence on q than q^2 approaching a q^3 dependence at some point. This transition region appears to occur over a broader q range for the HI than the no HI case. This behavior is also evident in Figure 1 but is much more transparent in Figure 5. At very large q, the HI curve exhibits oscillatory behavior that closely parallels the no HI curve. (In both cases, N, b_0, and c are the same.) As in the no HI case, the HI curve approaches plateau behavior with $K_1 = q^2D_s$.

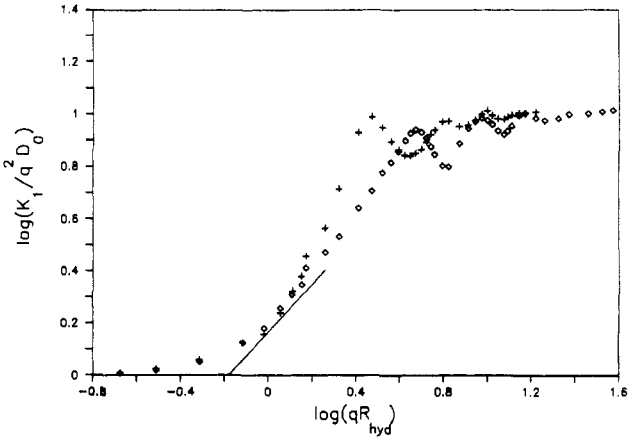

Figure 6. Effect of bending stiffness on K_1 for free draining, $N = 10$ chains. Solid line represents experimental cumulants. Diamonds correspond to $g = 1.31$ (same parameters as filled squares in Figure 1) while +'s correspond to $g = 0.0$ (same parameters as +'s in Figure 1).

Figure 6 illustrates the effect of bending stiffness on K_1 at large q. In this figure, HI is ignored, $N = 10$, $a = 46.7$ Å, and $c = 100$ in both cases, but $g = 1.31/0.0$ in the case of diamonds/crosses, respectively. Because of the constraint on $\langle S^2 \rangle$, b_0's are different in the two cases. At low q, the two curves are indistinguishable, but in the range $0.1 < \log(qR_{hyd}) < 0.4$, K_1 exhibits a stronger q dependence for the case with $g = 0$ than when $g = 1.31$. In fact, K_1 varies roughly with the 4th power of q in this range for $g = 0$ which is in fairly good agreement with the q^4 dependence expected for a free draining Rouse–Zimm chain. What these results suggest is that bending stiffness seems to reduce the power law dependence of K_1 on q from 4 to 3. This power law dependence also implies that light scattering should be sensitive to stiffness provided sufficiently high q values can be achieved. At very high q, both the $g = 0$ and 1.31 cases exhibit oscillatory behavior. The out of phase character is due to the fact different b_0's are used in the two models. Both cases converge to the same plateau behavior since the subunit radius is the same in both cases.

Figure 7 shows the effect of varying the stretching con-

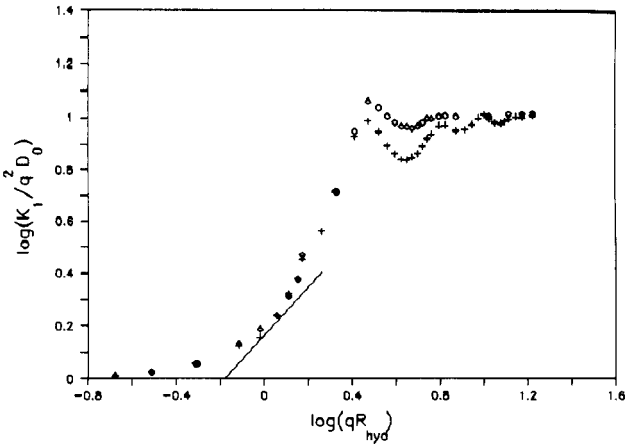

Figure 7. Effect of stretching stiffness on K_1 for free draining, $N = 10$ chains. Solid line represents experimental cumulants. Diamonds correspond to $c = 10$ (same parameters as diamonds in Figure 1) while +'s correspond to $c = 100$ (same parameters as +'s in Figure 1).

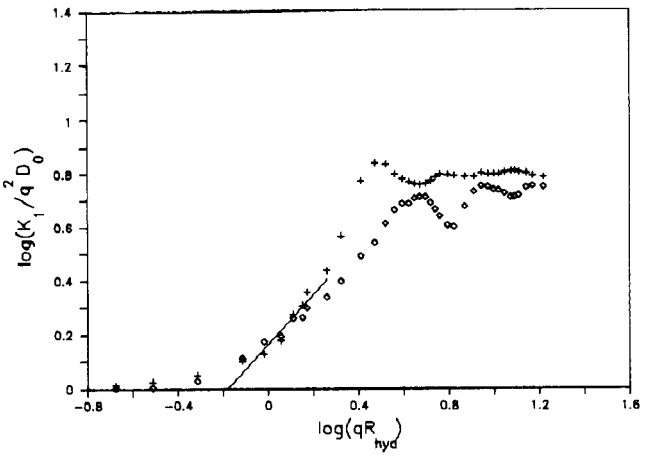

Figure 8. Effect of bending (and stretching) stiffness on K_1 for $N = 10$ chains with preaveraged hydrodynamic interaction. Solid line represents experimental cumulants. Diamonds represent stiff chains with $c = 100$ (same parameters as ×'s in Figure 1) while +'s represent flexible chains with $c = 10$ (same parameters as unfilled squares in Figure 1).

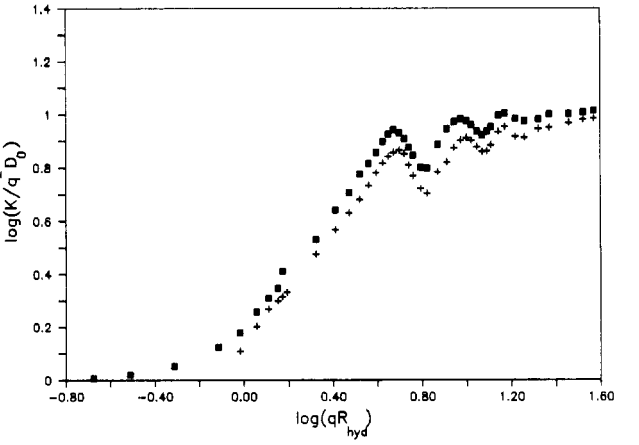

Figure 9. Comparison of K_1 and K_p for a free draining, $N = 10$ chain. Filled squares correspond to K_1 and +'s to K_p. Chain parameters are the same as the filled squares in Figure 1.

stant c. In both cases, $N = 10$, no HI, $g = 0$, and $a = 45.7$, but $c = 10/100$ for diamonds/crosses, respectively. Different b_0's are used although $\langle b^2 \rangle$ is the same in both. The only significant difference between the two cases occurs at large q, where the oscillatory behavior of the $c = 10$ case is attenuated relative to $c = 100$. The onset of oscillatory behavior in K_1 can be linked to the rms intersubunit separation in a quantitative way. Let q^* denote that scattering vector where $\log (K_1/q^2D_0)$ reaches its first maximum. It turns out $q^*\langle b^2 \rangle^{1/2} = 5.4$ to within 10% for all cases studied in this work. Reducing c reduces the amplitude of these oscillations, but for similar $\langle b^2 \rangle$, not the positions of the peaks and valleys. In order for a model to reproduce the cumulant behavior of an actual molecule up to some value of q, then the condition $q\langle b^2 \rangle^{1/2}$ less than about 4 must be satisfied. Another factor at large q concerns the breakdown of the "point scattering approximation" (see discussion following eq 16). It we assume this breakdown occurs at $qa = 1$, then upper bounds on $\log (qR_{hyd})$ of 1.30 and 0.76 can be established for $a = 23.6$ and 82 Å, respectively. Inspecting Figures 4–8 and accounting for the subunit radius associated with each data set, it can be seen that this upper bound does not occur until well into the oscillatory portion of K_1.

The effect of bending and stretching on K_1 with preaveraged HI is shown in Figure 8. In both cases, $N = 10$, but $g = 0/1.31$, $a = 77/82$ Å, $b_0 = 668/550$ Å, and $c = 10/100$ in the case of crosses/diamonds, respectively. As in the case of the free draining chains (Figure 6), stiffness appears to reduce the power law dependence of K_1 on q from roughly 4 ($g = 0$) to 3 ($g = 1.31$) over the range $0.2 < \log (qR_{hyd}) < 0.4$. This result for $g = 0$ is rather surprising since $K_1 \propto q^3$ for a long Rouse–Zimm chain. This discrepancy could be due, in part at least, to the small number of subunits in the chain that would have less hydrodynamic shielding than a long chain. It should also be noted from Figures 6 and 8 that the "linear" regime is much narrower for the flexible than for the stiff chains. In fact, the approach to plateau behavior for the $g = 0$ chains could very well be nonlinear on the basis of the figures.

Finally, shown in Figure 9 are K_1's (crosses) and K_p's (filled squares) for a particular free draining chain model. Although the two curves are slightly shifted relative to each other, they are otherwise very similar. These results indicate that K_p (obtained from average lifetime measurements[39–41]) should have about the same power law dependence on q as K_1.

IV. Summary

DLS has been very useful in studying translational motions of macromolecules. Even for flexible macromolecules like DNA, DLS at low q is only sensitive to translational motions. In general, however, the dynamic scattering form factor, $S(q,t)$, depends on the translational, rotational, and deformational motions in a complex way. Because of this, it is possible to use DLS to study these motions. In the past, the most frequently used procedures have involved cumulant[11,23,26,32] or average decay lifetime[15,39–41] fits of $S(q,t)$ over a range of q. These "single number" analyses have the advantage of simplicity, but they usually underutilize the data. Using a program such as CONTIN,[24] or others based on similar principles,[42,43] an attempt is made to actually reconstruct the distribution of lifetimes, $G(\tau)$, thereby gaining additional information.

In this work, Brownian dynamics simulation has been used to construct $S(q,t)$ for a number of different but very similar models. These correlation functions have then been analyzed by the "single number" approaches and by CONTIN. In the q range where experimental data is currently available, simulated and experimental cumu-

lants are in fairly good agreement provided the constraints of constant $\langle S^2 \rangle$ and D_0 are satisfied. (Simulations with preaveraged HI are essentially identical with those without preaveraging. This is consistent with previous work.[7,10] At $q^2 = 2.684 \times 10^{10}$ cm^{-2}, CONTIN analyses of simulations of 10 subunit chains with HI included are in better agreement with experiment than the corresponding free draining models. On the other hand, $G(\tau)$, K_1, and K_p seem to be fairly insensitive to changes in other model parameters in the experimentally accessible q range. In the case of $G(\tau)$, this insensitivity is due to fairly large uncertainties in the amplitudes and lifetimes of the faster decay processes, and the large uncertainties, in turn, are due to noise in the simulations. This uncertainty in $G(\tau)$ could be reduced by carrying out ensembles on significantly larger ensembles of chains. Unfortunately, however, computing time would increase proportionally.

Simulations at higher q are also reported. Out to $q \approx 5.0/\langle b^2 \rangle^{1/2}$, K_1 is independent of the number of beads comprising the chain. However, K_1 is sensitive to bending stiffness in this q region and varies roughly as q^3 (large g) to q^4 (small g) for free draining chains and chains with HI. At sufficiently large q, K_1 oscillates as a function of q and this oscillation is related to the mean-square separation of the subunits in the model. At extremely large q, K_1/q^2 reaches a plateau value determined by the subunit size. Both the oscillations and the existence of plateau diffusional behavior appear to be artifacts of the model and not characteristics of the macromolecule they represent. However, provided one only considers the regime $q < 5.0/\langle b^2 \rangle^{1/2}$, where $S(q,t)$ is insensitive to N and the artifacts discussed above are not present, we conclude that the general model used in this work serves as a realistic model for the actual macromolecule in its ability to mimick experimental light scattering behavior. It should be noted that light scattering measurements above q^2 of about 15×10^{10} cm^{-2} are difficult to perform.[44] Sample times are necessarily very short, and thus the number of photons per sample time are low. In order to obtain a signal-to-noise ratio comparable to measurements at lower q, long accumulation times must be carried out which is not always practical. Also, fluorescence and light absorption may become problems. DNA, for example, has an absorption maxima at 260 nm and a shoulder that extends out to about 300 nm. For a 300-nm light source and a scattering angle of 150°, $q^2 = 29.1 \times 10^{10}$ cm^{-2} (log $(qR_{hyd}) = 0.404$) which represents a realistic upper bound on q for this system on the basis of sample absorption.

Acknowledgment. S.A.A. would like to acknowledge NSF for a Presidential Young Investigator Award. S.S.S. and R.P. acknowledge NSF Grant CHE 8814611 and the NSF MRL program through the center for Materials Research at Stanford University.

References and Notes

(1) Fixman, M.; Kovac, J. *J. Chem. Phys.* **1989**, *90*, 2035.
(2) Ermak, D.; McCammon, J. A. *J. Chem. Phys.* **1978**, *69*, 1352.
(3) Fixman, M. *J. Chem. Phys.* **1988**, *89*, 2442.
(4) Helfand, E.; Wasserman, Z. R.; Weber, T. A. *Macromolecules* **1980**, *13*, 526.
(5) James, C.; Evans, G. T. *J. Chem. Phys.* **1982**, *76*, 2680.
(6) Allison, S. A.; McCammon, J. A. *Biopolymers* **1984**, *23*, 363.
(7) Allison, S. A. *Macromolecules* **1986**, *19*, 118.
(8) Lewis, R. J.; Allison, S. A.; Eden, D.; Pecora, R. *J. Chem. Phys.* **1988**, *89*, 2490.
(9) Allison, S. A.; Austin, R.; Hogan, M. *J. Chem. Phys.* **1989**, *90*, 3843.
(10) Rey, A.; Freire, J. J.; Garcia de la Torre, J. *J. Chem. Phys.* **1989**, *90*, 2035.
(11) Sorlie, S. S.; Pecora, R. *Macromolecules* **1988**, *21*, 1437.
(12) Pecora, R. *J. Chem. Phys.* **1965**, *43*, 1562; **1968**, *49*, 1032.
(13) Rouse, P. E., Jr. *J. Chem. Phys.* **1955**, *21*, 1272.
(14) Zimm, B. H. *J. Chem. Phys.* **1956**, *24*, 269.
(15) Lin, S.-C.; Schurr, J. M. *Biopolymers* **1978**, *17*, 425.
(16) Fujime, S.; Maruyama, M. *Macromolecules* **1973**, *6*, 237.
(17) Maeda, T.; Fujime, S. *Macromolecules* **1981**, *14*, 1981.
(18) Harris, R. A.; Hearst, R. E. *J. Chem. Phys.* **1966**, *44*, 2595.
(19) Hearst, J. E.; Harris, R. A.; Beals, E. *J. Chem. Phys.* **1966**, *45*, 3106; **1967**, *46*, 398.
(20) Soda, K. *J. Phys. Soc. Jpn.* **1973**, *35*, 866.
(21) Aragon, S. R.; Pecora, R. *Macromolecules* **1985**, *18*, 1868.
(22) Kratky, O.; Porod, G. *Recl. Trav. Chim. Pays-Bas* **1949**, *68*, 1106.
(23) Koppel, D. E. *J. Chem. Phys.* **1972**, *57*, 4814.
(24) Provencher, S. W. *Comp. Phys. Commun.* **1982**, *27*, 213, 229.
(25) Pecora, R. In *Dynamic Behavior of Macromolecules, Colloids, Liquid Crystals, and Biological Systems by Optical and Electro-Optical Methods*; Watanabe, H., Ed.; Hirokawa: Tokyo, 1989.
(26) Akcasu, A. Z.; Benmouna, M.; Han, C. C. *Polymer* **1980**, *21*, 866.
(27) Hagerman, P. J.; Zimm, B. H. *Biopolymers* **1981**, *20*, 1481.
(28) Bloomfield, V. A.; Crothers, D. M.; Tinoco, I., Jr. In *Physical Chemistry of Nucleic Acids*; Harper & Row: New York, 1974.
(29) Garcia de la Torre, J.; Jimenez, A.; Freire, J. J. *Macromolecules* **1982**, *15*, 148.
(30) Rotne, J.; Prager, S. *J. Chem. Phys.* **1969**, *50*, 4831.
(31) Berne, B. J.; Pecora, R. In *Dynamic Light Scattering*; Wiley: New York, 1976.
(32) Chu, B.; Dinapoli, A. In *Measurements of Suspended Particles by Quasi-Elastic Light Scattering*; Dahneke, B. E.; Ed.; Wiley: New York, 1983; p 81.
(33) Dubois-Violette, E.; de Gennes, P.-G. *Physics* **1967**, *3*, 181.
(34) Sorlie, S. S.; Pecora, R. *Macromolecules*, in press.
(35) Schaefer, D. W.; Han, C. C. In *Dynamic Light Scattering: Applications of Photon Correlation Spectroscopy*; Pecora, R., Ed.; Plenum: New York, 1985; p 181.
(36) Schurr, J. M. *Biopolymers* **1983**, *22*, 2207.
(37) Balabonov, S. M.; Ivanova, M. A.; Klenin, S. I.; Lomakin, A. V.; Molotkov, V. A.; Noskin, V. A. *Macromolecules* **1988**, *21*, 2528.
(38) Benight, A. S.; Langowski, J.; Wu, P-G.; Wilcoxon, J.; Shibata, J. H.; Fujimoto, B. S.; Ribeiro, N. S.; Schurr, J. M. In *Laser Scattering Spectroscopy of Biological Objects*; Stepanek, J., Anzenbacher, P., Seblacek, B., Eds.; Elsevier: Amsterdam, 1987; Vol. 45, p 407.
(39) Thomas, J. C.; Allison, S. A.; Schurr, J. M.; Holder, R. D. *Biopolymers* **1980**, *19*, 1451.
(40) Soda, K.; Wada, A. *Biophys. Chem.* **1984**, *20*, 185.
(41) Schurr, J. M.; Schmitz, K. S. *Annu. Rev. Phys. Chem.* **1986**, *37*, 271.
(42) Ostrowsky, N.; Sornette, D.; Parker, P.; Pike, E. R. *Opt. Acta* **1981**, *28*, 1059.
(43) Livesey, A. K.; Delaye, M.; Licinio, P.; Brochon, J.-C. *Faraday Discuss. Chem. Soc.* **1987**, *83*, 247.
(44) Thomas, J. C.; Schurr, J. M. *Opt. Lett.* **1979**, *4*, 222.